MEASUREMENTS ON HORIZONTAL BUOYANT JET IN CALM AMBIENT FLUID, WITH THEORY BASED ON VARIABLE COEFFICIENT OF ENTRAINMENT DETERMINED EXPERIMENTALLY

by H.O. ANWAR

Dr.-Ing. - Principal Scientific Officer
Hydraulics Research Station, Wallingford,
Berks (England).

Introduction

The flow pattern of a buoyant jet (forced plume) discharging from a horizontal nozzle into a stagnant fluid is rather complex. In order to tackle this type of plume theoretically it has been suggested, and confirmed experimentally, that its behaviour at a certain distance from the nozzle is like a convectional plume above a point source, when the diameter of the nozzle relative to the vertical reach of the plume is very small.

The behaviour of a forced plume near the nozzle is dominated mainly by its initial momentum, which reduces en route due to the entrainment of the ambient fluid and the plume becomes more and more under the influence of the buoyancy force. The writer has shown previously [3, 4] that the calculated trajectory and the dilution along it, based upon the above suggestion, agree reasonably well with the measured data for the values of densimetric Froude numbers (defined by Eq. 6) less than ten occuring mostly in the practice, when the assumption is made that the forced plume behaves as a simple plume from the end of its potential core. The length of the potential core of a momentum jet is between six and eight times the nozzle diameter.

This paper is concerned with certain measurements on forced plumes issuing horizontally into a calm ambient fluid, which so far as the writer is aware, have not been carried out previously by the writer [3] and the others [1, 7] for their theoretical approaches. Moreover, it has been found that the results of the theoretical approach based upon the theory of convectional plumes does not agree with the results obtained from experiment of the buoyant jet when the densimetric Froude number (Eq. 6) is larger than ten. A better agreement has been obtained from the modified theory for the case considered here. Warm water at a temperature of about 58 °C was discharged from a horizontal nozzle of 1/2 in. diameter into ambient fresh water at a temperature of about 11 °C. Temperatures and the temperature fluctuations, (within the limit of the thermistor sensitivity) have been measured at various sections perpendicular to the axis of the plume. Further tests have been conducted to measure the velocity along the trajectory of the plumes and also to determine the width of the plume. The investigation was carried out for various densimetric Froude numbers based upon the nozzle diameter, ranging from 5 to 16.

Experimental arrangement

The experiments were conducted in a transparent walled flume 30 ft long, 5 ft wide and 3 ft high. The flume was closed at both ends and was filled with fresh water at a temperature of about 11 °C, to a height of 24 in. above the nozzle. The nozzle of 1/2 in. diameter was placed horizontally at a distance of 8 in. above the bottom of the flume in order to exclude its effect on the plume. Warm water was supplied from a storage tank with a capacity of 10^3 cubic feet, and it was heated to the desired temperature with a 39 kW immersion heater. A one cusec pump provided thorough mixing of the warm water before it

was used in the experiments. The warm water discharge through the nozzle was registered by a "Rotameter" calibrated for the above given temperature. The temperature and its fluctuation were measured with a thermistor, of type, F, obtained from Standard Telephone & Cables Ltd. The time constant of the thermistor, which is that taken to respond to $(e-1)/e \approx 0.63$ ($e = 2.7183$) of a step change in temperature, was measured and found to be about 1/4 s when it was immersed in well agitated water. The thermistor was connected to a data-logger. The data-logger was in turn connected to a punched paper tape output, which recorded ten samples in a second. The time for taking samples at each point of the plume varied between 70 to 90 s. The results of sampling at points near the edge and the centre of the plume are shown for example in Figure 1. This figure indicates that if high frequencies of temperature fluctuation exist, the thermistor does not respond to them. As a result of the limited speed of response, the measured r.m.s. value of the temperature may be lower than its actual value. The r.m.s. and the mean values of the temperature were then evaluated from the punched tape by the use of a digital computer. The above values have been evaluated by calculating arithmetic mean value as well as integrated over the time given above. The results of these two types of evaluation have been compared.

The velocity along the axis of the plume was measured photographically. A cine camera was positioned in the front of the flume and the lighting was provided from the rear of the flume. By placing a temporary square grid at the middle of the flume, i.e. the centre plane of the plume, and photographing it through the front wall of the flume, which was also marked with a reference grid, the scale of the photography was obtained. To trace the rising plume photographically, a Methylene Blue organic dye with a concentration of 40 ppm was used. The solution was warmed up to the desired temperature and injected into the pipe connected to the nozzle.

The trajectory of the plume was then determined from the developed film. With the appropriate scaling factor the number of the frames per each division gave length-time curves for various nozzle densimetric Froude numbers which is expressed by Equation (6). The mean values of velocities along the trajectory of the plume have been calculated as described later from the length-time curves.

Experimental results

The mean values of temperature at each point have been computed from the punched tape according to the following equations:

$$T_1 = \frac{1}{N}\sum_{h=1}^{N} t_h \tag{1}$$

$$T_2 = \frac{1}{\tau}\int_{\tau_0}^{\tau_0+\tau} t_h d\tau \tag{2}$$

and the following equations have been used to calculate the root-mean-square values:

$$\theta_1 = \left(\overline{t_1'^2}\right)^{1/2} = \left[\frac{1}{N}\sum (t_h - T_1)^2\right]^{1/2} \tag{3}$$

$$\theta_2 = \left(\overline{t_1'^2}\right)^{1/2} = \left[\frac{1}{\tau}\int_{\tau_0}^{\tau_0+\tau} (t_h - T_2)^2 d\tau\right]^{1/2} \tag{4}$$

In the above Equations T_1 and T_2 are the values of the mean temperature, and θ_1 and θ_2 are measures of their fluctuations. τ is the total time for taking N number of digitized data at each point. The computer programme for the evaluation of Equations (2) and (4) was written by using Simpson's rule. Hence, as to be expected, the values of T_1 and T_2 and also values of θ_1 and θ_2 were almost the same after 50 s.

For instance $T_1 = 17.1760784$, $T_2 = 17.1759659$ °C, $\theta_1 = 1.6716366$ and $\theta_2 = 1.6714557$ °C when $\tau = 50$ s. Therefore only Equations (1) and (3) have been used for evaluation of the measured temperature.

It was mentioned before that the time for taking the sample by thermistor at each point was between 70 and 90 s. The variation of the mean temperature and its fluctuation with the duration of the sampling period can be seen in Figure 2. This figure shows that the measured data remains almost unchanged when time, τ, is about 70 s.

Mean temperature profile

Mean temperature profiles across the section of the plume were measured and evaluated at various distances from the end of potential core. The results are shown in dimensionless form for the lefthand side of the trajectory in Figure 3. In this figure r_L is the radial distance from the axis of the plume, and δ_L is a relevant radius scale, given by $r_L = \delta_L$ where the temperature excess $(T_e - T_a)$ is half of that which occurs at the axis of the plume. T_e is the temperature at any point along the radius r_L and T_a is the ambient temperature (Fig. 4). These profiles which were measured in the turbulent region of the plume, were found to be geometrically similar and a good empirical fit to them can be given by the following expression:

$$\frac{T_e - T_a}{T_m - T_a} = \exp\left[-0.693\left(\frac{r_L}{\delta_L}\right)^2\right] \tag{5}$$

where T_m is the temperature at the axis of the plume. Figure 5 shows the results of the above-mentioned evaluation for the righthand side (Fig. 4) of the plume-axis. It can be seen that in Figure 5 there are less measured data and also more scatter of the points than in Figure 3, because of the difficulties inherent in the experiments, as will be explained below.

When the radii were determined for those points in the measured temperature profiles for which the amplitude of the temperature excess was 0.1 of the excess on the axis of the plume, it was found that except near the nozzle and the free surface, these radii were shorter on the righthand side than on the left. This indicates that the assumption of circular sections for the plume under consideration is not true except near the nozzle and the free surface. The righthand side profiles thus gave a steeper gradient for the temperature distribution, and hence more measurements needed to be taken on these parts in order to obtain an accurate distribution. Unfortunately this was not appreciated during the measurements, and is probably a cause of the apparent scatter on Figure 5. Figures 3 and 5 verify the assumption that was made by the writer and other researchers [1, 5] in their theoretical approach that the profiles of density at various sections for the plume under consideration can be treated as being of Gaussian form; making allowances for the non-linear relationship between the temperature and density with water as a test fluid.

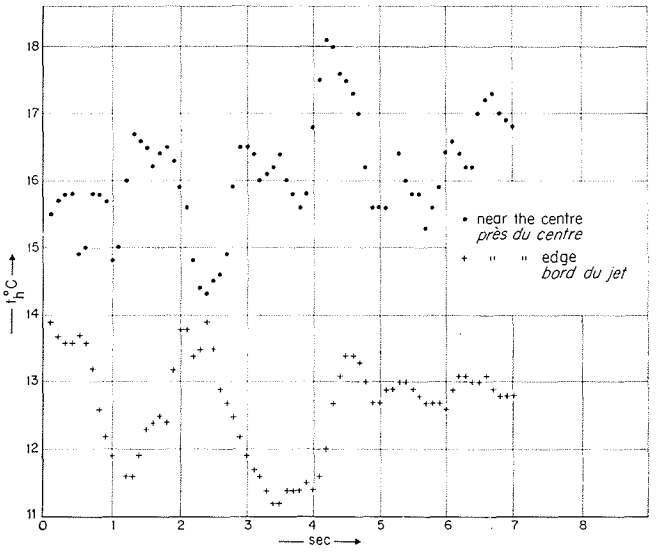

1/

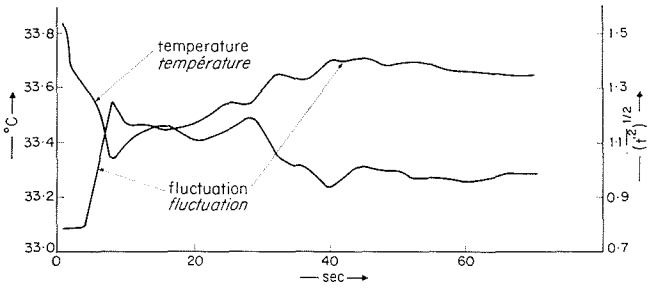

2/

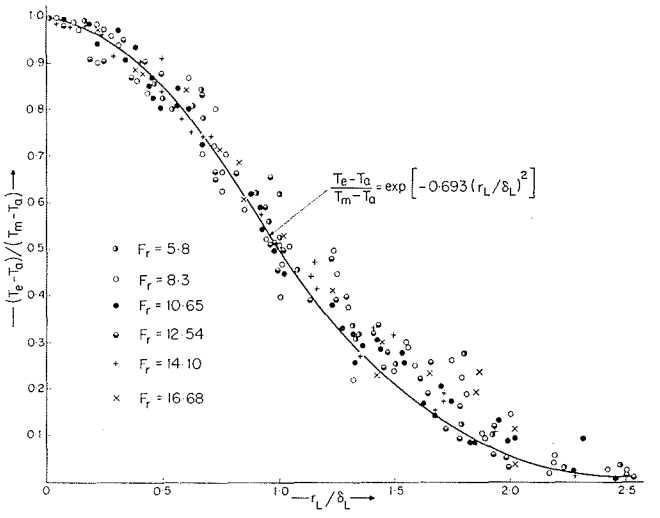

3/

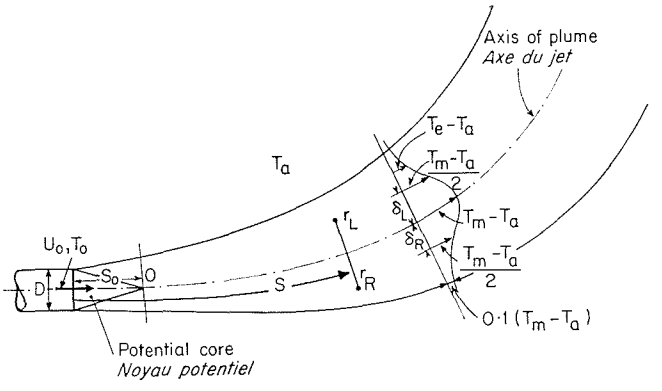

4/

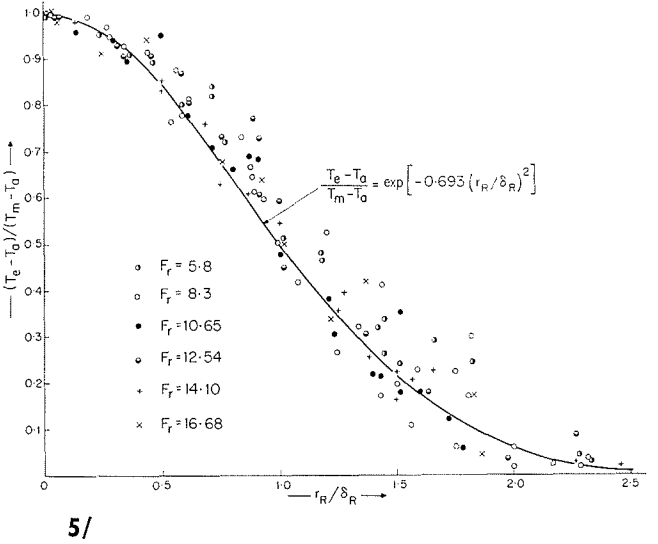

5/

1/ Temperature records obtained with thermistor.
Enregistrements de température obtenus par thermistance.

2/ Variation of mean temperature and r.m.s. value of temperature with duration of sampling at $r_R = 0.25$ in and $F_r = 14.1$.
Moyenne et valeur quadratique moyenne de la température en fonction de la durée des relevés ($r_R = 0{,}25''$, $F_r = 14{,}1$).

3/ Mean temperature profile of the left-hand side of the plume for various sections at distance S.
Profil moyen de température du côté gauche du panache pour diverses sections à la distance S.

4/ Definition of terms for the rising plume.
Définition des termes se rapportant au panache.

5/ Mean temperature profile of the right-hand side of the plume for various sections at distance S.
Profil moyen de température du côté droit du panache pour diverses sections à la distance S.

It was mentioned previously that the r.m.s. values of temperature fluctuation were calculated by Equation (3). These data, for nozzle densimetric Froude numbers 5.8, 8.3 and 10.65, are shown as turbulent intensity of temperature fluctuation in Figure 6 for various sections at distance S (Fig. 4) along the trajectory. The nozzle densimetric Froude number in this paper was calculated according to the following expression:

$$F_r = U_0 / \left(g \frac{\rho_a - \rho_0}{\rho_a} D \right)^{1/2} \quad (6)$$

in which U_0 is the mean velocity of warm water at the nozzle exit, ρ_0 is the density of warm water at the nozzle exit, ρ_a is the density of the ambient water and D is the nozzle diameter. Within the limit of experimental scatter and considering that the thermistor was not sensitive enough (as described before) for the temperature fluctuations, Figure 6 shows that the self-preservation of the distribution of turbulent intensity of temperature fluctuation is attained. However Figure 6 together with Figure 3 and 5 supports the assumption of self-preserving flows [3] for the plume under consideration. Figure 6 further shows that the measured profiles became distorted when $S > 7.6$. This means a steeper gradient of the mean temperature distribution in the region at the righthand side of the centre-line.

Velocity

Velocity along the trajectory has been evaluated by two different methods. As described before, the length S of the trajectory has been plotted against time, in order to obtain length-time curve, for various nozzle densimetric Froude numbers. The angle between the tangent to the length-time curves and the time-axis at each point gives the velocity at the points. The second method, which was considered to be more accurate than the first one, was to fit several least square parabolas to each length-time curve, section by section with the condition that the parabolas overlap each other at several points. It was found that this method gave computed length-time curves, which passed through the measured data reasonably well. Hence the derivative gave the velocity at any points in the fitted region. The first method gave velocities which are scattered around the velocity curves obtained by the second method. However, the results of the measured velocities for various values of F_r are shown in Figure 7. In it are also shown theoretical curves, calculated from the following equation, for comparison:

$$\frac{U_m}{U_0} = \frac{1}{F} \frac{M}{\Delta} = \frac{\lambda}{(2.3)^{1/4} \alpha^{1/2}} \frac{1}{F_r} \frac{M}{\Delta} \quad (7)$$

in which M is the non-dimensional momentum flux, Δ is non-dimensional flux, λ is a non-dimensional parameter representing the ratio of sideway spread between the velocity and the density profiles as is equal to 1.16 determined experimentally, α is the coefficient of entrainment assumed to be constant and equal to 0.082 and finally F is a source densimetric Froude number which refers to Section 0 (Fig. 4). The values of M and Δ can be calculated from the system of Equations (21) (23) given by the writer [3]. In Figure 7 the length S_0, which is the length of the potential core (see Figure 4), was taken to be equal to about 7.5 D [3] ($S_0 = 7.5$ and $D = \frac{1}{2}$ in.) and the velocity U_0 for each F_r can be seen in table 1.

Table 1

F_r	U_0 (in/sec)
5.8	9
8.3	13.77
10.65	17.81
12.54	21.3
14.1	24.00
16.68	28.6

Figure 7 shows that in a region beyond S_0 the measured data deviate considerably from the theoretical curves based upon the theory of convectional plumes.

Hence the shortcoming of the theory for this region is obvious for a rising plume emitted from a horizontal nozzle. The theoretical approach is modified to produce a better agreement as discussed later.

Plume-width

From the temperature profiles, which were measured at various distances S, the radii δ_L and δ_r were determined. It was then assumed that the temperature profile is of Gaussian form i.e. :

$$\frac{T_c - T_a}{T_m - T_a} = \exp\left[-\left(\frac{r_{r,L}}{\lambda b} \right)^2 \right] \quad (8)$$

from the above expression the width, b, of the plume can be written as follows:

$$b = \frac{\delta_{r,L}}{0.833\,\lambda} \quad (9)$$

The calculated b-values for a given F_r were plotted against S on transparent paper, at which the film, described before, was superimposed. It was then observed that there exists a dye-front in the plume advancing faster than any part of the plume. The dye-front moves on the theoretical trajectory [3], which agrees with the experimental one obtained from temperature measurements. The calculated boundary from Equation (9) was filled with dye very quickly as the dyefront was advancing. It was further observed that on the outside of the plume boundary there is a zone of less dye-intensity when the dye-front reaches the free surface. The width of the plume was measured from the transparent paper at various distance S and the results are shown in Figure 8. In this figure is also shown the theoretical curves for comparison. The theoretical curves can be obtained from the following equation:

$$\frac{b}{D} = \frac{F}{(2.3)^{1/2}} \frac{\Delta}{M^{1/2}} = \frac{\alpha^{1/2} F_r}{(2.3)^{1/4} \lambda} \frac{\Delta}{M^{1/2}} \quad (10)$$

The terms on the righthand side of the above equation were defined before. Figure 8 shows that reasonable agreement between calculation and measurements can be found when :

$$(S - S_0)/D > 10$$

The theoretical curves show that the width of the plume grows, at first rapidly and then slowly, whereas the experimental curve grows almost linearly in the transition zone.

Coefficient of entrainment α

In order to determine the coefficient α from the measured data the following method has been adapted. It may seem to be rather crude but, at least, gives some indication of its variation. The statement expressing the conservation of mass within the control volume can be written as follows:

$$\frac{d}{d\,(S-S_0)} \int U dA = \oint_c U_i dc \qquad (11)$$

where A denotes the area and c the circumference of the control volume, U_i is the velocity of the ambient fluid entrained by the plume and U is the local velocity.

By accepting the assumption made elsewehe [3, 5 and 6] that $U_i = \alpha U_m$, it has been shown experimentally that the coefficient α is constant both for a vertical simple plume and for jets [6, 7]. But this is not the case for the plume considered here [2, 3]. Here it will be assumed that it is at least constant along a small portion of the trajectory. Hence we can write Equation (11) in the following form by introducing into it the Gaussian forms for the velocity and the density distribution [3].

$$\frac{d}{d\,(S-S_0)} (U_m b^2) = 2\,\alpha\, b U_m \qquad (12)$$

where b is the width of the plume. From Equation 11 the following expression can be obtained for α:

$$\alpha = \frac{d\,(U_m\, b^2)/d\,(S-S_0)}{2\, b U_m} \qquad (13)$$

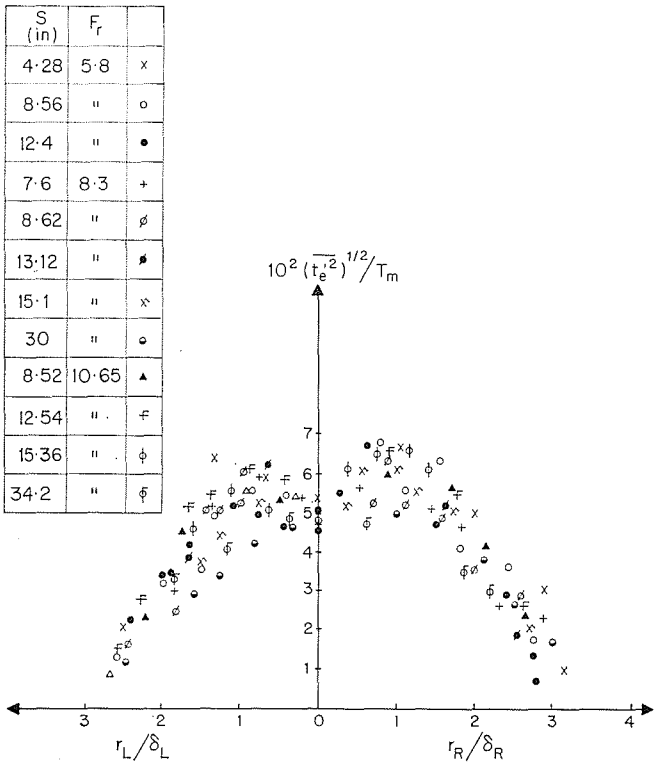

6/ Profiles of turbulent intensity of temperature fluctuation for various F_r values.

Profils de l'intensité turbulente des fluctuations de température pour diverses valeurs de F_r.

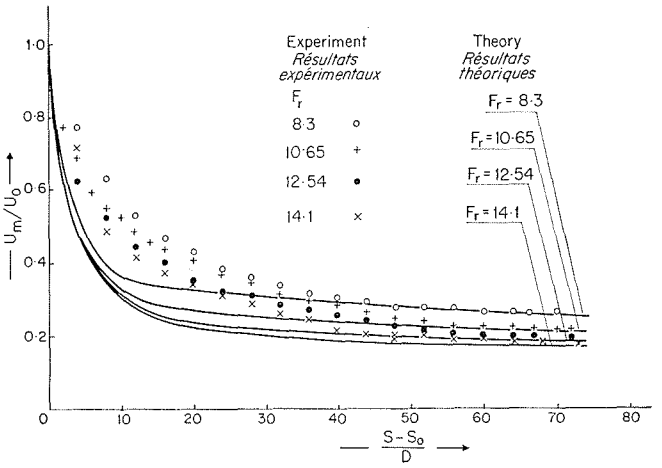

7/ Velocity distribution along the plume axis.

Distribution des vitesses le long de l'axe du panache.

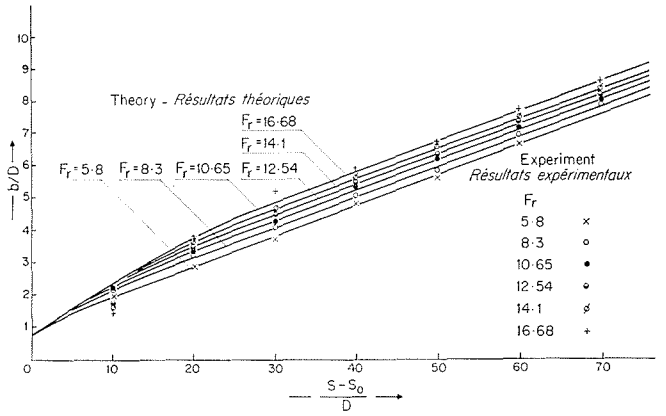

8/ Width of buoyant jet.

Largeur du jet.

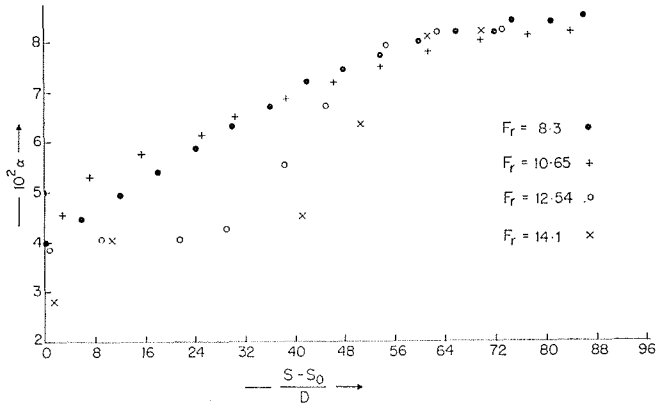

9/ Variation of entrainement coefficient with non-dimensional distance of the plume axis.

Coefficient d'entraînement en fonction de la distance réduite à l'axe du panache.

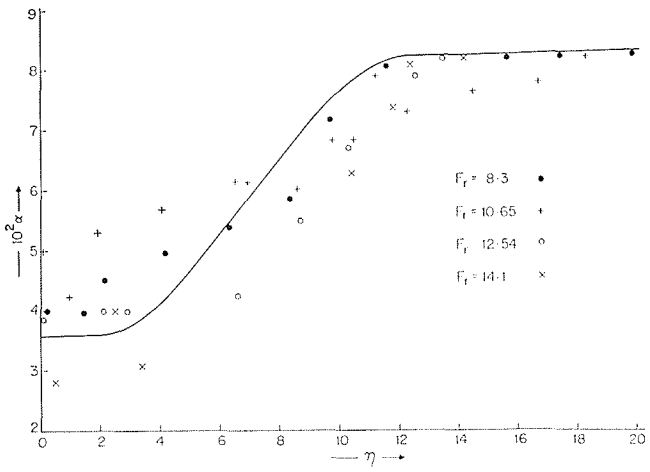

10/ Variation of α with non-dimensional distance.
α en fonction de la distance réduite.

The numerator of Equation (13) has been computed from the curves passing through the points obtained by plotting the experimental values of b^2U_m against $S - S_0$ for various F_r. Then the values of α at various distances $S - S_0$ have been calculated from Equation (13). The results of the calculation are given in Figure 9, in which the values of α are plotted against non-dimensional distance $(S - S_0)/D$ for various F_r. The points are rather scattered, with the results for $F_r = 8.3$ and $F_r = 10.65$ exhibiting more consistent behaviour. The value of α reaches 0.082 at the later stage. This value of α was used in the earlier theoretical approach [3]. Figure 9 generally shows an increase of α when $(S - S_0)/D$ increases. The results shown in Figure 9 should be accepted with reserve, and more experimental work is necessary to establish their validity.

Modified theory of buoyant jet in stagnant ambient fluid

It was pointed out by the author [3] that the phenomena in a convectional plume (simple plume) from a point source does not depend on Richardson's number based on the sectional mean value of velocity and density differences (the reciprocal of the local densimetric Froude number), since no work is required to be done against gravity. But this is not true, particularly in the curved region, for a buoyant jet emitted horizontally. It can be concluded therefore, that the coefficient of entrainment α, introduced prévious-ly [3] as a constant into the equation for conservation of volume, is variable. Moreover Figure 9 shows that the coefficient α varies with non-dimensional distance $(S - S_0)/D$ and it approaches almost a constant value when:

$$(S - S_0)/D > 52$$

This can also be seen in Figure 7 in which the measured data for velocity deviates considerably from the theory based upon constant α when $(S - S_0)/D < 40$. On the other hand it can be argued that the apparent deviation in Figure 7 is due to the initial momentum, which has not been considered in the theoretical approach for this region. If the last assumption is true the value of α in Figure 9 should then start with $\alpha = 0.057$, which is the appropriate value for the coefficient of entrainment for a momentum jet, and not with a value less than 0.04.

In this section, however, the theoretical approach given before [3] has been modified to take into account the variation of α along the plume axis.

The equations for conservation of volume, of momentum and of mass deficiency for a rising plume used by the author [3] are:

$$\frac{d}{d(S - S_0)}(b^2U_m) = 2\,\alpha b U_m \tag{14}$$

$$\frac{d}{d(S - S_0)}(b^2U_m^2) = 2\,g\,\frac{\rho_a - \rho_m}{\rho_a}(\lambda b)^2 \sin\theta \tag{15}$$

$$b^2U_m^2\,\frac{d\theta}{d(S - S_0)} = 2\,g\,\frac{\rho_a - \rho_m}{\rho_a}(\lambda b)^2 \cos\theta \tag{16}$$

$$\frac{d}{d(S - S_0)}\left[g(\rho_a - \rho_m)\,U_m b^2\right] = 0 \tag{17}$$

in which ρ_m is the density at the axis of the plume, and θ is the angle of inclination of the tangent to the plume-axis. The boundary conditions of the above equations are:

$$b = b_0\,,\ \frac{\rho_a - \rho_m}{\rho_a} = \frac{\rho_a - \rho_0}{\rho_a}\,,$$
$$U_0 = U_m\,,\ \theta = 0 \quad \text{at} \quad S' = S - S_0 = 0 \tag{18}$$

The non-dimensional parameters:

$$S^0 = 2\,\frac{S'}{b_0}\,,\ b^0 = \frac{b}{b_0}\,,$$

$$B = \frac{g\,\dfrac{\rho_a - \rho_m}{\rho_a}}{g\,\dfrac{\rho_a - \rho_0}{\rho_a}}$$

and:

$$U^0 = \left[\frac{1}{\lambda^2}\,\frac{1}{b_0}\,\frac{\rho_a}{g(\rho_a - \rho_0)}\right]^{1/2} U_m \tag{19}$$

transfer equations (14-17) to the following form:

$$\frac{d}{dS^0}(b^{0^2}U^0) = \alpha\, b^0 U^0 \tag{20}$$

$$\frac{d(b^{0^2}U^{0^2})}{dS^0} = B b^{0^2} \sin\theta \tag{21}$$

$$b^{0^2}U^{0^2}\,\frac{d\theta}{dS^0} = B b^{0^2} \cos\theta \tag{22}$$

$$B b^{0^2} U^0 = F = \left[\frac{1}{\lambda^2}\,\frac{1}{b_0}\,\frac{\rho_a}{g(\rho_a - \rho_0)}\right]^{1/2} U_0 \tag{23}$$

Subject to the boundary conditions:

$$b^0 = 1,\ U^0 = F,\ B = I,\ \theta = 0 \text{ at } S^0 = 0 \tag{24}$$

By introducing the following new variables:

$$b^{0^2}U^0 = F^2\Delta,\ b^{0^2}U^{0^2} = F^2M,\ S^0 = F\eta \tag{25}$$

into equations (20) - (22) the following equations are obtained:

$$\frac{d\Delta}{d\eta} = \alpha M^{1/2} \tag{26}$$

$$\frac{dM}{d\eta} = \frac{\Delta}{M} \sin\theta \qquad (27)$$

$$M \frac{d\theta}{d\eta} = \frac{\Delta}{M} \cos\theta \qquad (28)$$

subject to the boundary conditions:

$$\Delta = \frac{1}{F}\ ,\ M = 1,\ \theta = 0 \text{ at } \eta = 0$$

The relation between F and F_r can be given in the following form [3]:

$$F = \frac{(2.3)^{1/4}}{\lambda} F_r \qquad (29)$$

In Equation (26) the coefficient α varies with η. In order to determine this functional variation the measured data given in Figure 9 has been plotted against η in Figure 10 by using Equation (25). The solid line shown in this figure has been used for a numerical computer programme to solve equations (26) (28). The results of this solution are compared with those obtained from the assumption of constant $\alpha = 0.082$ for the entire plume. The following relation has been used for the computation [3], [5] i.e.:

$$D = \sqrt{2}\, b_0 \qquad (30)$$

and $\lambda = 1.16$ as was given before.

The results of this comparison are shown in Figure 11, in which the non-dimensional ordinate has been calculated according to the following equation:

$$\frac{y}{D} = \frac{F}{2^{3/2}} \int_1^M \frac{(M^2 - 1)}{M}\, d\eta \qquad (31)$$

which can be obtained from Equation (30) and the relationship given in Reference [3].

In Figure 11 the term C_0/C_m [3] represents the dilution along the plume axis defined as follows:

$$C_0/C_m = \frac{\rho_a - \rho_0}{\rho_a - \rho_m} = F\Delta \qquad (32)$$

Figure 11 shows that the dilution along the plume-axis obtained from the above analysis (Equations (27-28) agrees with that calculated from the theory based on constant α when $F_r < 10$ and the agreement occurs for much less than ten for $C_0/C_m = 10$. Figure 11 further shows that the dilution C_0/C_m calculated from the above analysis is more, hence longer trajectory, than that calculated from the theory based on constant α when $F_r > 10$. This can be seen in Figure 12, in which are shown the trajectories of a plume of $F_r = 20$ obtained from various theoretical approaches [1, 3, 5] and also calculated from the above analysis. The non-dimensional abscissa in Figure 12 has been calculated according to the following equation [3]:

$$\frac{x}{D} = \frac{F}{2^{3/2}} \int_1^M \frac{(M^2 - 1)^{1/2}}{M}\, d\eta \qquad (33)$$

In Figure 12 are also shown the experimental results for comparison. This figure shows that the above analysis agrees reasonably with the measurements and also with the analyses given by Abraham [1], which is also based upon the variation of α along the plume axis by assuming that the buoyant jet behaves as a momentum jet near the nozzle and as a simple plume near the surface. This assumption, however, does not agree entirely with the experimental results shown in Figure 10. Further comparison is made between calculations and measurements in table 2, which shows good agreement between the results of present analysis and the measurements. Table 2 shows

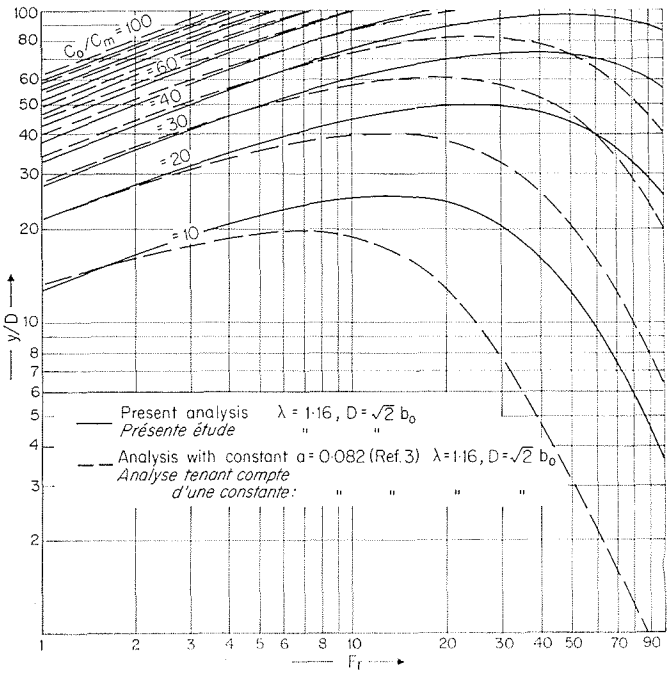

11/ Dilution along the plume axis.

Dilution le long de l'axe du panache.

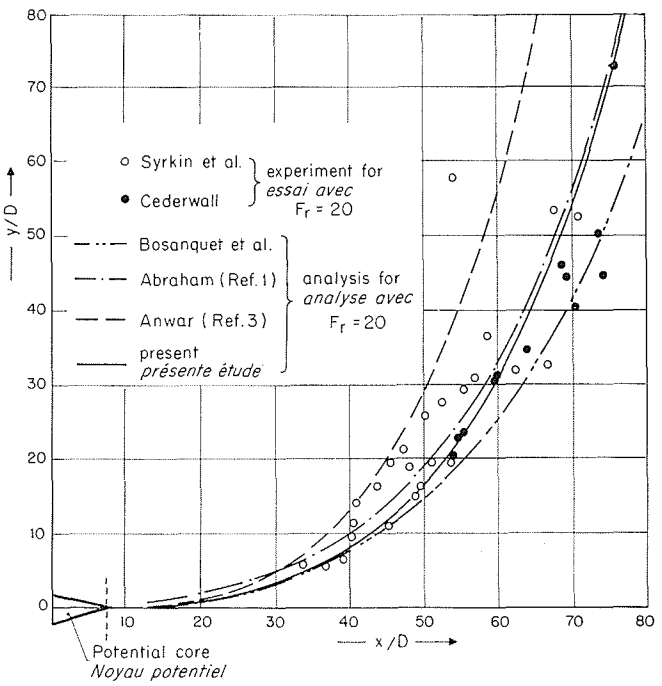

12/ Trajectory of buoyant jet for $F_r = 20$ obtained from various theoretical approaches.

Trajectoire du jet ascendant à $F_r = 20$ selon diverses théories.

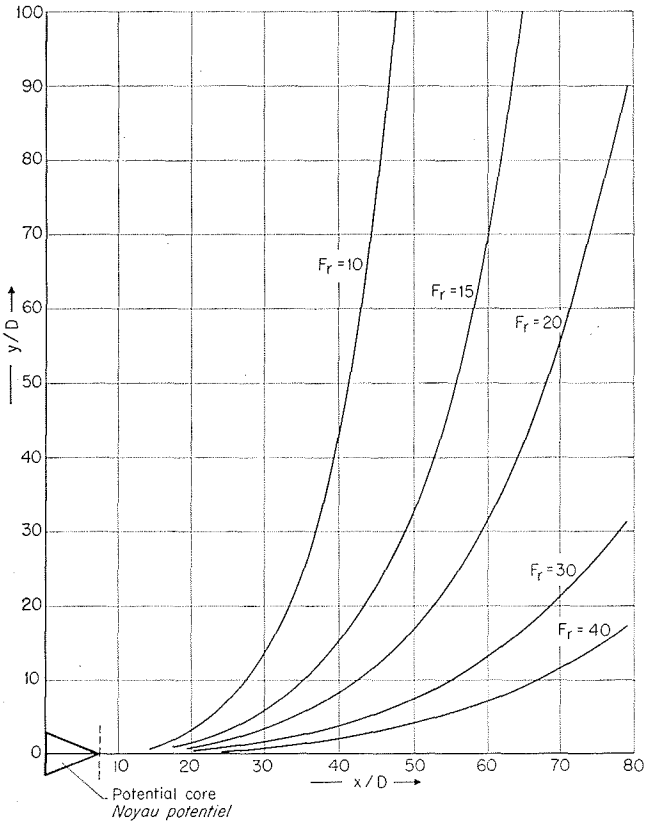

13/ Trajectory of buoyant jet for $F_r \geqslant 10$ obtained from present therory.

Trajectoire du jet ascendant à $F_r \geqslant 10$ d'après la théorie présente.

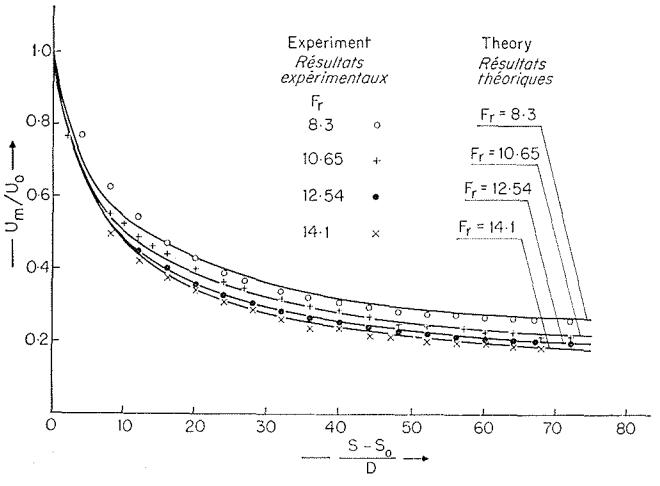

14/ Velocity distribution along the plume-axis obtained from present theory.

Distribution des vitesses le long de l'axe du panache selon la théorie présente.

that the results of the theory based on constant coefficient of entrainment agree reasonably well with those obtained from measurements when $F_r < 10$. (This will be discussed later.) The experimental results shown in the table are in good agreement with the results obtained from present analysis when $F_r > 10$. Hence for the practical purposes the trajectory of the buoyant jet, by using Equations (26 - 28) together with Equations (31) and (33), for various densimetric Froude number, F_r, are shown in Figure 13.

Table 2

F_r	Experiment (Ref. 8)		Present Analysis	
	x/D	y/D	x/D	y/D
8.60	27.4	17.6	28.95	17.6
17.4	48.1	18.6	46.6	18.6
23.4	53.6	13.3	51.34	13.3
30.6	45.1	3.86	40.88	3.86
34.9	75.2	13.3	66.62	13.3
41.4	79.7	11.42	71.55	11.42

F_r	Abraham's analysis (Ref. 1)		Analysis with constant α	
	x/D	y/D	x/D	y/D
8.60			26.82	17.6
17.4	43.4	18.6	41.4	18.6
23.4	48.7	13.3	44.6	13.3
30.6	37.1	3.86	36.2	3.86
34.9	63.65	13.3	57.05	13.3
41.4			60.6	11.42

Moreover the x/D and y/D values obtained from the experiment presented here were also close to those given in table 2.

The measured velocity along the plume axis was compared with the calculated velocity from the present theory. The results of this comparison are shown in Figure 14. This figure shows that the measured data agrees reasonably well with the theoretical curves.

Figures 11, 12 and 13 indicate that the buoyant jet moves vertically upwards almost immediately beyond the termination of potential core (Fig. 4) when the densimetric Froude number is less than ten. In this case the buoyant jet behaves as a simple plume and coefficient of entrainment α should be considered as a constant equal to 0.082 for the entire region.

Acknowledgments

The work described herein was carried out as part of a research programme of the Hydraulics Research Station and the paper is published by permission of the Director of Hydraulics Research. The writer wishes to express his thanks to Mr. J.A. Weller for his help in measurement and also to Mr. P.J. Harden who did the computer work.

References

[1] ABRAHAM (G.). — Horizontal jets in stagnant fluid of other density. *Journal of the Hydraulics Division, A.S.C.E.*, vol. 91, N° HY 4, Proc. paper 4411 (July 1965), p. 139-154.

[2] ABRAHAM (G.). — Entrainment principle and its restriction to solve problems of jets. *Journal of Hydraulics Research*, N° 2 (1965), p. 1-23.

[3] ANWAR (H. O.). — Behaviour of buoyant jet in calm fluid. *Journal of the Hydraulics Division, A.S.C.E.*, vol. 95, N° HY 4, Proc. paper 6688 (July 1969), p. 1289-1303.

[4] ANWAR (H. O.). — Experiment on an effluent discharging from a slot into stationary or slow moving fluid of greater density. *Journal of Hydraulics Research*, N° 47 (1969), p. 411-431.

[5] BOSANQUET (C. H.)., HORN (G.) and THRING (M. W.). — The effect of density differences on the path of jets. *Proceedings Royal Society*, Series A, vol. 263, (sept. 1961), p. 340-352.

[6] CEDERWALL (K). — Hydraulics of marine waste water disposal. Sweden Report N° 42, Hydraulic Division, *Chalmers Institute of Technology*, Gotebörg, (January 1968).

[7] FAN (L. N.) and BROOKS (N. H.). — Discussion of Horizontal jets in stagnant fluid of other density, by Abraham (G.). *Journal of the Hydraulics Division, A.S.C.E.*, vol. 92, n° HY 2, Proc. paper 4708, (March 1966), p. 423-429.

[8] HANSON (J.) and SCHRODER (H.). — Horizontal jet dillusion studies by use of radioactive isotopes. *Acta Polytechnica Scandinavica, Civil Eng. and Building Construction*, Series N° 49, (Copenhagen, 1968).

[9] MORTON (B. R.), TAYLOR (G. I.) and TURNER (J. S.). — Turbulent Gravitational Convection from maintained and instantaneous source. *Proceedings, Royal Society*, Series A, vol. 234, (January 1956), p. 1-23.

[10] RICOU (F. P.) and SPALDING (D. B.). — Measurements of entrainment by axisymmetrical turbulent jet. *Journal of Fluid Mech.*, vol. 11, (1961), p. 21-32.

[11] SYRKIN (A. N.) and LYAKHOVSKIY (D. N.). — Aeronautics of an elementary flame, (1936), see also Reference [1].

Résumé

Etude expérimentale d'un jet qui débouche horizontalement dans un fluide plus lourd au repos et comparaison avec une étude théorique fondée sur un coefficient d'entraînement variable mesuré expérimentalement

Diverses caractéristiques d'un panache ascendant d'eau chaude injectée horizontalement dans de l'eau plus froide au repos ont été déterminées par l'expérience. La valeur du nombre de Froude faisant intervenir la différence de densités et défini par rapport au diamètre de la buse d'injection, varie entre 5,8 et 16. Les fluctuations de température de nature turbulente sont mesurées durant 70 à 90 s, à la cadence de dix relevés par seconde. Ces mesures ont eu lieu dans diverses sections du panache et en divers points de chaque section. La température moyenne ainsi que la valeur quadratique moyenne des fluctuations sont déterminées à partir des relevés.

Les résultats montrent que la température est normalement distribuée mais que la section du panache n'est circulaire qu'à proximité de la buse ou de la surface libre. On a déterminé pour diverses sections la distribution de la valeur quadratique moyenne de la température. Ces résultats tendent à confirmer la validité de la théorie de similitude proposée.

Sont également mesurées : la vitesse moyenne le long de la trajectoire et la largeur du panache. Les résultats sont en assez bon accord avec la théorie modifiée fondée sur le panache convectif qui se forme sur une source chaude.

Le coefficient d'entraînement a également été déterminé à partir des mesures. Lorsque la distance à la buse s'accroît, la valeur du coefficient augmente jusqu'à environ 0,082. D'autres expériences sont cependant nécessaires pour confirmer cette valeur.